

# TURBULENT DISPERSION IN POROUS MEDIA MODELED AS AN INFINITE ARRAY OF LONGITUDINALLY-DISPLACED ELLIPTIC RODS

**Marcos Heinzemann Junqueira Pedras**

Instituto de Pesquisa e Desenvolvimento IP&D, UNIVAP  
12244-000, São José dos Campos, SP, Brasil. E-mail: pedras@univap.br

**Francisco D. Rocamora Jr.**

Instituto de Estudos Avançados - IEAv/CTA  
12231-970, São José dos Campos-SP, Brazil. E-mail: rocamora@mec.ita.br

**Marcelo J.S. De-Lemos \***

Departamento de Energia - IEME  
Instituto Tecnológico de Aeronáutica - ITA

\* Corresponding author. 12228-900, São José dos Campos, SP, Brasil. E-mail: delemos@mec.ita.br

**Abstract.** Thermal dispersion in porous media is an important phenomenon in combustion and in steam injection systems for Enhanced Oil Recovery methods. Accordingly, the study of flow through porous media has gained much attention lately and advances in proper modeling of such flows, which includes non-linear effects, have been published. In this work, thermal dispersion tensors were calculated within an infinite porous medium formed by a spatially periodic array of longitudinally-displaced elliptic rods. For the sake of simplicity, just one unit-cell, together with periodic boundary conditions for mass and momentum equations, and Neumann and Dirichlet conditions for the temperature equation, was used to represent such medium. The numerical methodology herein employed is based on the control-volume approach. Turbulence is assumed to exist within the fluid phase and a low Reynolds  $k-\epsilon$  model is used to model such non-linear effects. The flow equations at the pore-scale were numerically solved using the SIMPLE method on a non-orthogonal boundary-fitted coordinate system. The integrated results were compared to the existing data presented in the literature.

**Keywords:** porous media, thermal dispersion, periodic boundary conditions, low Reynolds  $k-\epsilon$  model, macroscopic energy equation.

## 1. Introduction

Due to its great application in the industry and science, the study of the flow in porous media has received great attention lately and advances in proper modeling of such flows, including non-linear effects, have been published (Pedras and de Lemos, 2001a; de Lemos and Pedras, 2001; Rocamora and de Lemos, 2000; Pedras and de Lemos, 2001b; Pedras and de Lemos, 2001c; Pedras *et al.*, 2003; Pedras and de Lemos, 2003). Engineering systems based on fluidized bed combustion, enhanced oil reservoir recovery, combustion in an inert porous matrix, underground spreading of chemical waste and chemical catalytic reactors are just a few examples of such applications. In some of these applications the thermal dispersion in porous media is an important phenomenon, in which one has used (Hsu and Cheng, 1990; Kaviany, 1995; Ochoa-Tapia and Whitaker, 1997; Moyne, 1997; Quintard *et al.*, 1997; Kuwahara and Nakayama, 1998; Nakayama and Kuwahara, 1999) the notion of a Representative Elementary Volume (REV, Fig. 1) for the mathematical treatment of governing equations. These models, based on the macroscopic point of view, lose details on the flow pattern inside the REV and, together with ad-hoc information, provide global flow properties such as average velocities and temperatures.

Such flows can also be analyzed by modeling the topology of the porous medium and resolving the flow equations at the pore-scale. This treatment reveals the flow structure at the pore-scale level and was used by (Quintard *et al.*, 1997; Kuwahara and Nakayama, 1998; Nakayama and Kuwahara, 1999; Rocamora and de Lemos, 2002) to calculate the thermal dispersion tensors with periodic boundary condition for the mass, momentum and the energy equations.

The aim of the present contribution is to discuss the modeling of thermal dispersion and calculate the thermal dispersion tensors within an infinite porous medium formed by spatially periodic array of longitudinally-displaced elliptic rods. For the sake of simplicity, just one unit-cell, together with periodic boundary conditions for mass and momentum equations, and Neumann and Dirichlet conditions for the temperature equation, was used to represent such medium. Turbulence is assumed to exist within the fluid phase and a low Reynolds  $k-\epsilon$  model is used to model such non-linear effects.

The flow equations at the pore-scale were numerically solved using the SIMPLE method on a non-orthogonal boundary-fitted coordinate system. The integrated results were compared to the existing data presented in the literature.

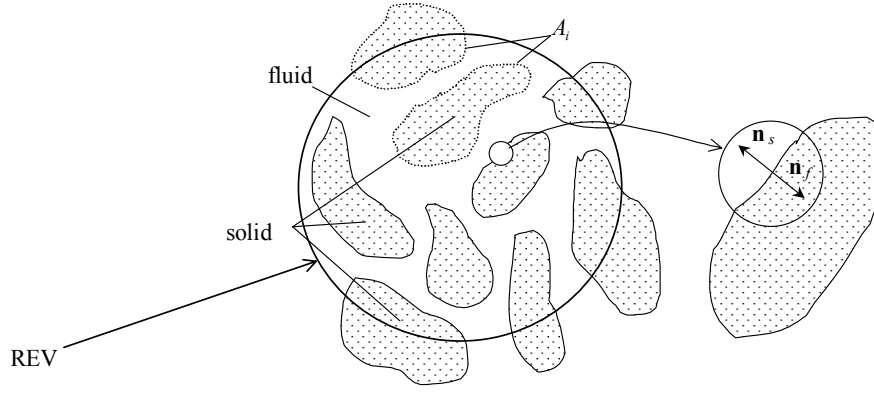


Figure 1. Representative elementary volume (REV).

## 2. Microscopic Equations

The following microscopic transport equations describe the flow field and the heat transfer process within a porous medium, where barred quantities represent time-averaged components and primes indicate turbulent fluctuations:

Fluid Phase (incompressible fluid):

$$\nabla \cdot \bar{\mathbf{u}} = 0 \quad (1)$$

$$\rho_f \left[ \frac{\partial \bar{\mathbf{u}}}{\partial t} + \nabla \cdot (\bar{\mathbf{u}} \bar{\mathbf{u}}) \right] = -\nabla \bar{p} + \nabla \cdot \{ \mu [\nabla \bar{\mathbf{u}} + (\nabla \bar{\mathbf{u}})^T] - \rho_f \overline{\mathbf{u}' \mathbf{u}'} \} \quad (2)$$

$$\rho_f c_{pf} \left[ \frac{\partial \bar{T}_f}{\partial t} + \nabla \cdot (\bar{\mathbf{u}} \bar{T}_f) \right] = \nabla \cdot [k_f \nabla \bar{T}_f - \rho_f c_{pf} \overline{\mathbf{u}' T'_f}] \quad (3)$$

$$\rho_f \left[ \frac{\partial k}{\partial t} + \nabla \cdot (\bar{\mathbf{u}} k) \right] = \nabla \cdot \left[ \left( \mu + \frac{\mu_t}{\sigma_k} \right) \nabla k \right] - \rho_f \overline{\mathbf{u}' \mathbf{u}'} : \nabla \bar{\mathbf{u}} - \rho_f \varepsilon \quad (4)$$

$$\rho_f \left[ \frac{\partial \varepsilon}{\partial t} + \nabla \cdot (\bar{\mathbf{u}} \varepsilon) \right] = \nabla \cdot \left[ \left( \mu + \frac{\mu_t}{\sigma_\varepsilon} \right) \nabla \varepsilon \right] + [C_1 (-\rho_f \overline{\mathbf{u}' \mathbf{u}'} : \nabla \bar{\mathbf{u}}) - C_2 f_2 \rho_f \varepsilon] \frac{\varepsilon}{k} \quad (5)$$

$$-\rho_f \overline{\mathbf{u}' \mathbf{u}'} = \mu_t [\nabla \bar{\mathbf{u}} + (\nabla \bar{\mathbf{u}})^T] - \frac{2}{3} \rho_f k \mathbf{I} \quad (6)$$

$$-\rho_f c_{pf} \overline{\mathbf{u}' T'_f} = \rho_f c_{pf} \frac{\nu_t}{\sigma_t} \nabla \bar{T}_f \quad (7)$$

$$\mu_t = \rho_f \nu_t = \rho_f C_\mu f_\mu \frac{k^2}{\varepsilon} \quad (8)$$

Solid Phase:

$$\rho_s c_{ps} \frac{\partial \bar{T}_s}{\partial t} = \nabla \cdot [k_s \nabla \bar{T}_s] \quad (9)$$

where  $\mathbf{u}$  is the microscopic velocity,  $\rho_f$  and  $\rho_s$  the fluid and solid densities,  $p$  the thermodynamic pressure,  $\mu$  and  $\mu_t$  the dynamic and turbulent viscosities,  $T_f$  and  $T_s$  the fluid and solid temperatures,  $c_{pf}$  and  $c_{ps}$  the fluid and solid specific heat at constant pressure,  $k_f$  and  $k_s$  the fluid and solid thermal conductivities,  $k$  the turbulent kinetic energy and  $\varepsilon$  the dissipation of  $k$ . In the equations,  $\sigma_k$ ,  $\sigma_\varepsilon$  and  $\sigma_t$  are effective Prandtl numbers,  $C_1$ ,  $C_2$  and  $C_\mu$  are dimensionless constants and  $f_2$  and  $f_\mu$  damping functions.

In this work the use of the low Re  $k$ - $\varepsilon$  model is justified by the fact that the turbulent flow in porous media occurs for Reynolds numbers (based on the pore) relatively low. To account for the low Reynolds effects, the following damping functions and model constants were adopted (Abe *et al.*, 1992):

$$f_2 = \left\{ 1 - \exp \left[ - \frac{(v\varepsilon)^{0.25} n}{3.1\nu} \right] \right\}^2 \times \left\{ 1 - 0.3 \exp \left[ - \left( \frac{k^2/v\varepsilon}{6.5} \right)^2 \right] \right\} \quad (10)$$

$$f_\mu = \left\{ 1 - \exp \left[ - \frac{(v\varepsilon)^{0.25} n}{14\nu} \right] \right\}^2 \times \left\{ 1 + \frac{5}{(k^2/v\varepsilon)^{0.75}} \exp \left[ - \left( \frac{k^2/v\varepsilon}{200} \right)^2 \right] \right\} \quad (11)$$

$$C_\mu = 0.09, C_1 = 1.5, C_2 = 1.9, \sigma_k = 1.4, \sigma_\varepsilon = 1.3. \quad (12)$$

For the unit-cell represented in Fig. (2) and with the assumption of macroscopic fully developed uni-dimensional flow, the boundary conditions are given as follow:

$$\text{at the walls, } \bar{\mathbf{u}} = 0; \bar{T}_f = \bar{T}_s; \mathbf{n}_f \cdot (k_f \nabla \bar{T}_f) = -\mathbf{n}_s \cdot (k_s \nabla \bar{T}_s); k = 0 \text{ and } \varepsilon = \nu \frac{\partial^2 k}{\partial n^2}, \quad (13)$$

on  $x=0$  and  $x=H$  periodic boundaries (momentum equation),

$$\bar{u}|_{x=0} = \bar{u}|_{x=H}, \bar{v}|_{x=0} = \bar{v}|_{x=H}, k|_{x=0} = k|_{x=H} \text{ and } \varepsilon|_{x=0} = \varepsilon|_{x=H} \quad (14)$$

on  $y=0$  and  $y=H$ ,

$$\frac{\partial \bar{u}}{\partial y} = \frac{\partial \bar{v}}{\partial y} = \frac{\partial k}{\partial y} = \frac{\partial \varepsilon}{\partial y} = 0 \quad (15)$$

where  $n_f$  and  $n_s$  are the coordinates normal to the interface (Fig. 1) and  $u$  and  $v$  the components of  $\mathbf{u}$ .

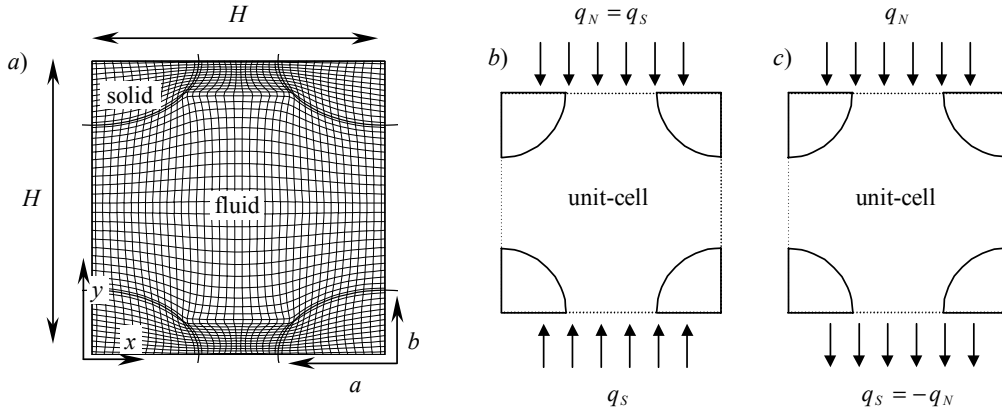


Figure 2. Unit-cell: a) elliptically generated grid ( $a/b=5/3$ ), b) and c) Neumann boundary conditions for the temperature  $k_f \frac{\partial \bar{T}}{\partial y} = k_s \frac{\partial \bar{T}}{\partial y} = -q$ .

The temperature boundary conditions will be presented in the next section.

### 3. Thermal Dispersion Modeling

Using the double decomposition concept (Pedras and de Lemos, 2001a) of a general quantity  $\phi_\beta$  in the  $\beta$  phase,

$$\phi_\beta = \langle \bar{\phi}_\beta \rangle^\beta + {}^i \bar{\phi}_\beta + \langle \phi'_\beta \rangle^\beta + {}^i \phi'_\beta \quad (16)$$

and following the procedure of Rocamora and de Lemos (2000) and Rocamora and de Lemos (2002), the volume averaging of the energy equations (3) and (9) over the REV, assuming local thermal equilibrium between the solid and fluid phases, namely  $\langle \bar{T}_f \rangle^f = \langle \bar{T}_s \rangle^s = \langle \bar{T} \rangle$ , renders:

$$[\phi_f \rho_f c_{pf} + \phi_s \rho_s c_{ps}] \frac{\partial \langle \bar{T} \rangle}{\partial t} + \rho_f c_{pf} \nabla \cdot (\langle \bar{\mathbf{u}} \rangle \langle \bar{T} \rangle) = \nabla \cdot \mathbf{K}_{eff} \cdot \nabla \langle \bar{T} \rangle \quad (17)$$

where  $\langle \varphi_\beta \rangle$  is the volume average of  $\varphi_\beta$ ,  $\langle \varphi_\beta \rangle^\beta$  the intrinsic average of  $\varphi_\beta$  in the  $\beta$  phase,  $\varphi'_\beta$  the time fluctuation of  $\varphi_\beta$ ,  ${}^i\varphi_\beta$  the space deviation of  $\varphi_\beta$ ,  $\phi_f$  the volume fraction of fluid and  $\phi_s = 1 - \phi_f$  the volume fraction of solid. The effective conductivity,  $\mathbf{K}_{eff}$ , the tortuosity tensor,  $\mathbf{K}_{tor}$ , and the dispersion tensor,  $\mathbf{K}_{dis}$ , are defined as:

$$\mathbf{K}_{eff} = \left( \phi_f \frac{\rho_f c_{pf} V_{t\phi}}{\sigma_t} + \phi_f k_f + \phi_s k_s \right) \mathbf{I} + \mathbf{K}_{tor} + \mathbf{K}_{dis} \quad (18)$$

$$\mathbf{K}_{tor} \cdot \nabla \langle \bar{T} \rangle = \frac{(k_f - k_s)}{\Delta V} \int_{A_i} \mathbf{n}_f {}^i\bar{T}_f dS \quad (19)$$

$$\mathbf{K}_{dis} \cdot \nabla \langle \bar{T} \rangle = -\rho_f c_{pf} \phi_f \langle {}^i\bar{\mathbf{u}} {}^i\bar{T}_f \rangle^f = -\frac{\rho_f c_{pf}}{\Delta V} \int_{\Delta V_f} {}^i\bar{\mathbf{u}} {}^i\bar{T}_f dV \quad (20)$$

If one introduces a linear relationship between the temperature deviation and the gradient of the average temperature,

$${}^i\bar{T}_f = \mathbf{b}_f \cdot \nabla \langle \bar{T} \rangle \quad (21)$$

the tortuosity tensor (19) and the thermal dispersion tensor (20) can be rewritten as:

$$\mathbf{K}_{tor} = \frac{(k_f - k_s)}{\Delta V} \int_{A_i} \mathbf{n}_f \mathbf{b}_f dS \quad (22)$$

$$\mathbf{K}_{dis} = -\frac{\rho_f c_{pf}}{\Delta V} \int_{\Delta V_f} {}^i\bar{\mathbf{u}} \mathbf{b}_f dV \quad (23)$$

It is interesting to point out that for a fixed macroscopic flow and temperature conditions in a periodic medium, Eqs. (19) and (20) show that the tortuosity and thermal dispersion tensors will be constant only if the temperature deviation field is periodic (repeated in each unit-cell). The deviation concept,  $\bar{T}_f = \langle \bar{T} \rangle + {}^i\bar{T}_f$ , confirms that the temperature deviation field is periodic in a periodic medium with a constant  $\nabla \langle \bar{T} \rangle$ . In this condition the temperature,  $\bar{T}_f$ , will change of  $\nabla \langle \bar{T} \rangle$  from a unit-cell to the next adjacent one, the average temperature  $\langle \bar{T} \rangle$  will undergo the same change and, therefore, the temperature deviation,  ${}^i\bar{T}_f$ , will remain the same (periodic).

On the other hand, if one uses the liner relationship (21) and calculates the tortuosity and thermal dispersion tensors via Eqs. (22) and (23), an equation for the  $\mathbf{b}_f$  vector is necessary (for details concerning its derivation, see *e.g.* Kaviani, 1995). This equation is independent of the temperature, *i.e.*, the  $\mathbf{b}_f$  vector depends only on the flow field and morphology of the medium and consequently tortuosity and thermal dispersion tensors will be independent of the temperature imposed on the porous medium. This fact occurs due to the linear hypothesis used for the temperature deviation (21). To avoid the consequences of the linear hypothesis we used Eq. (20) for calculating the thermal dispersion tensor.

If the gradient of the average temperature is in the same direction of the macroscopic flow or transverse to it, only diagonal components of  $\mathbf{K}_{dis}$  remain non-zero components. In these conditions, Eq. (20) renders the longitudinal component of  $\mathbf{K}_{dis}$ ,

$$(K_{dis})_{xx} = \frac{-\rho_f c_{pf}}{\frac{\Delta V}{H}} \int_{\Delta V_f} {}^i\bar{u} {}^i\bar{T}_f dV \quad (24)$$

$$(K_{dis})_{yy} = \frac{-\rho_f c_{pf}}{\frac{\Delta V}{H}} \int_{\Delta V_f} {}^i\bar{v} {}^i\bar{T}_f dV \quad (25)$$

In Eqs. (24) and (25) the gradients  $\Delta\langle\bar{T}\rangle_x$  and  $\Delta\langle\bar{T}\rangle_y$  can be calculated in two ways. The first one is using the Neumann boundary conditions sketched, respectively, in Figs (2b and 2c). In this case  $\Delta\langle\bar{T}\rangle_x$  and  $\Delta\langle\bar{T}\rangle_y$  are given as,

$$\Delta\langle\bar{T}\rangle_x = \frac{1}{H} \int_{y=0}^{y=H} [\bar{T}_{x=H} - \bar{T}_{x=0}] dy \quad \text{and} \quad \Delta\langle\bar{T}\rangle_y = \frac{1}{H} \int_{x=0}^{x=H} [\bar{T}_{y=H} - \bar{T}_{y=0}] dx \quad (26)$$

The second way is using Dirichlet boundary conditions (Kuwahara and Nakayama, 1998 and Rocamora and de Lemos, 2001) for the energy equation,

$$\bar{T}_{x=0} = \bar{T}_{x=H} - \Delta\langle\bar{T}\rangle_x \quad \text{and} \quad \bar{T}_{y=0} = \bar{T}_{y=H} \quad (27)$$

for the  $(K_{dis})_{xx}$  calculation, and,

$$\bar{T}_{x=0} = \bar{T}_{x=H} \quad \text{and} \quad \bar{T}_{y=0} = \bar{T}_{y=H} - \Delta\langle\bar{T}\rangle_y \quad (28)$$

for the  $(K_{dis})_{yy}$  calculation. In this case  $\Delta\langle\bar{T}\rangle_x$  and  $\Delta\langle\bar{T}\rangle_y$  are constants.

#### 4. Numerical Model

The governing equations were discretized using the finite volume procedure, Patankar (1980). The SIMPLE algorithm for the pressure-velocity coupling was adopted to correct both the pressure and the velocity fields. The process starts with the solution of the two momentum equations. Then the velocity field is adjusted in order to satisfy the continuity principle. This adjustment is obtained by solving the pressure correction equation. After that, the turbulence model equations and the energy equation are relaxed to update the  $k$ ,  $\varepsilon$  and temperature fields. Details on the numerical discretization can be found in Pedras and de Lemos (2001b).

For a fixed flow and the Neumann temperature conditions (Fig. 2b, c) the thermal dispersion tensors were calculated after a sequence of converged loops on the same run. This sequence of loops is necessary for the temperature field development, whereas for the velocity field this is not necessary because of the periodic boundary conditions used. The temperature development was carried out using the outlet temperature of a loop as the inlet temperature for the next loop. This procedure is repeated until we have no change in the temperature deviation field.

In the low Re model, the node adjacent to the wall requires that  $u_\tau n / \nu \leq 1$ . To accomplish this requirement, the grid needs points close to the wall leading to computational meshes of  $40 \times 54$  nodes. A highly nonuniform grid arrangement was employed with concentration of nodes close to the wall. Values for  $(K_{dis})_{xx}$  and  $(K_{dis})_{yy}$  were obtained varying the  $Pe_H = |\langle\bar{\mathbf{u}}\rangle| H / \alpha_f$  from  $10^0$  to  $4.10^3$  and the  $\phi_f = 1 - ab\pi/H^2$ , from 0.60 to 0.90.

#### 5. Results and Discussion

A total of twenty seven runs were carried out being twenty three for laminar flow and four for turbulent flow with the low Re model theory. In all runs it was used for the fluid phase a Prandtl number of 0.72 and a ratio of the solid phase thermal conductivity to fluid phase  $k_s/k_f = 2$ .

Figure (3) presents the temperature fields calculated with the temperature boundary conditions sketched in Fig. (2b), while Fig. (4) presents the temperature fields in the same flow rate but using the temperature boundary conditions Eq. (27). In both figures, the gradients of the average temperature are in the same direction of the macroscopic flow. As will be shown further, in spite of the differences in the temperature fields obtained, the values of the longitudinal component of  $\mathbf{K}_{dis}$  were very similar. Furthermore, Figs. (3b and 4b) show that as the flow rate is increased the fluid phase temperature become uniform, due to the mixing produced in the flow.

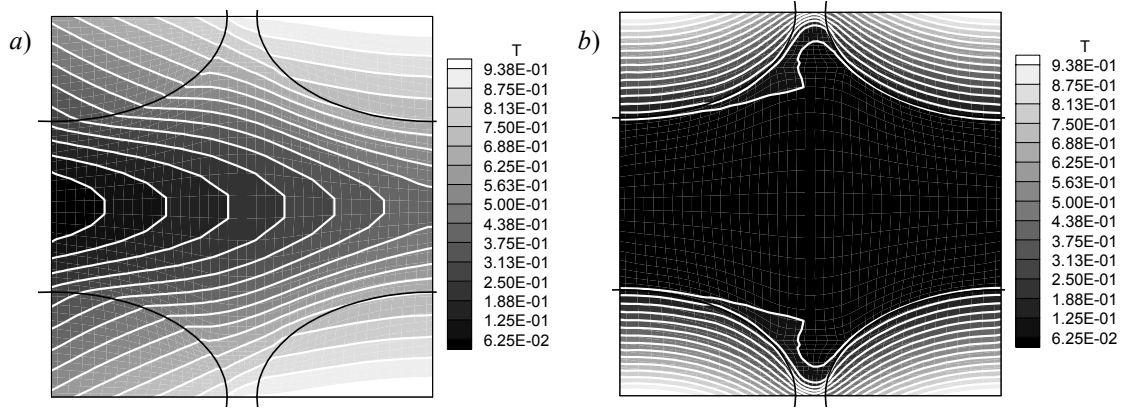


Figure 3. Temperature fields calculated with the temperature boundary conditions sketched in Fig. (2b) and  $\phi_f = 0.60$ : a)  $Pe_H = 10$ , and b)  $Pe_H = 4 \times 10^3$ .

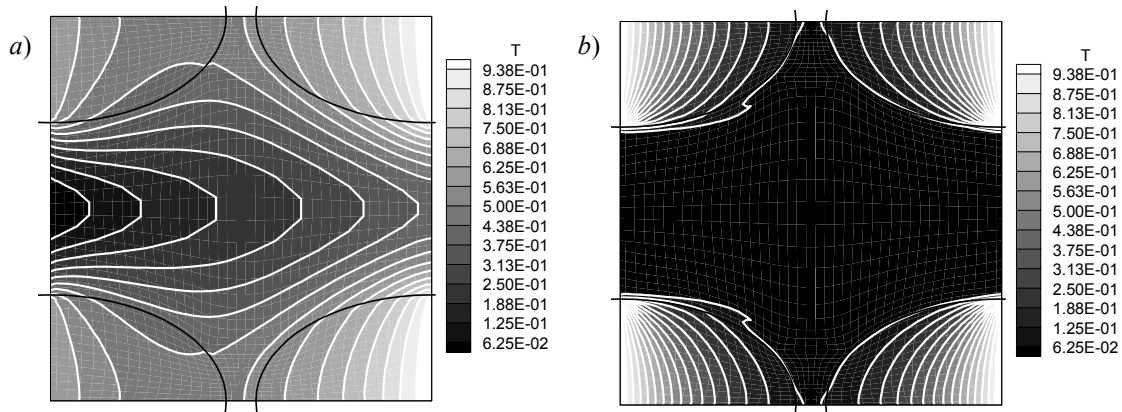


Figure 4. Temperature fields calculated with the temperature boundary conditions Eq. (27) and  $\phi_f = 0.60$ : a)  $Pe_H = 10$ , and b)  $Pe_H = 4 \times 10^3$ .

Figures (5 and 6) present the temperature fields calculated, respectively, with the temperature boundary conditions sketched in Fig. (2c) and with Eq. (28), which yield a gradient of the average temperature transverse to the macroscopic flow. In both cases, the temperature fields shown are very close each other and, consequently, the transversal component of  $\mathbf{K}_{dis}$  were very similar. Figures (5b and 6b) show the same behavior of Figs. (3b and 4b), *i.e.*, as the flow rate is increased the fluid phase temperature become uniform, due the mixing produced in the flow.

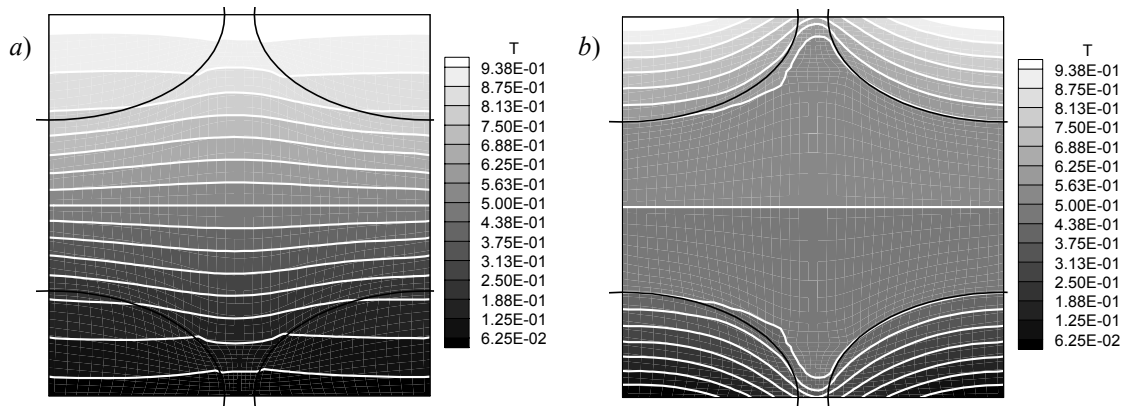


Figure 5. Temperature fields calculated with the temperature boundary conditions sketched in Fig. (2c) and  $\phi_f = 0.60$ : a)  $Pe_H = 10$ , and b)  $Pe_H = 4 \times 10^3$ .

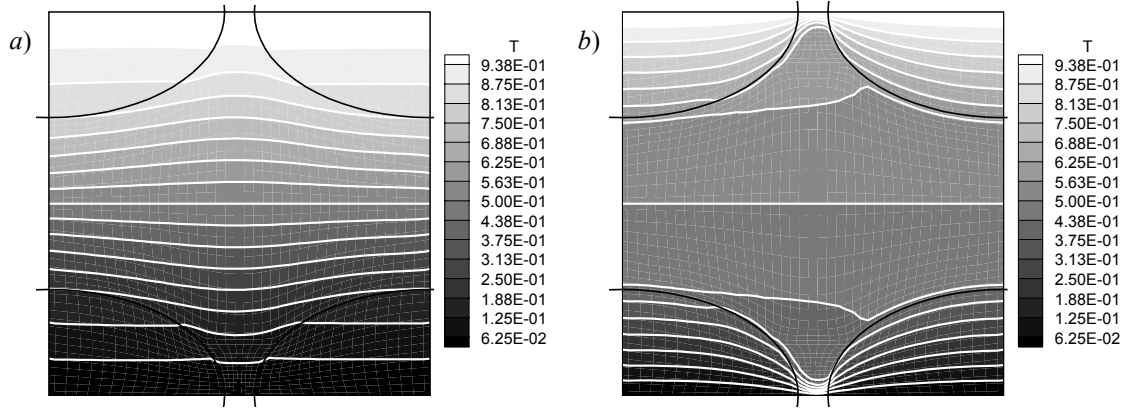


Figure 6. Temperature fields calculated with the temperature boundary conditions Eq. (28) and  $\phi_f = 0.60$ : a)  $Pe_H = 10$ , and b)  $Pe_H = 4 \times 10^3$ .

The longitudinal component of the thermal dispersion tensor is shown in Fig. (7) as a function of Peclet number and for different porosities. The results present good agreement when compared with the data of Kuwahara and Nakayama (1998) and Rocamora and de Lemos (2001), for square and cylindrical rods, respectively. The present results show that the use of different temperature boundary conditions (Fig. 2b and Eq. 27) yields very little differences in the values of the longitudinal component. Furthermore, for the longitudinal component, different morphologies (elliptical, square and cylindrical) also change very little its values. Its overall dependence on the Peclet number was  $(K_{dis})_{xx}/k_f = 0.056Pe_H^{1.6}$ , showing the usual behavior of  $(\sim Pe_H^n)$  as expected. The power dependence on the Peclet number of about 1.6 was lower than the square dependence of Taylor dispersion in a tube. This behavior can be ascribed to the turbulence, which contributes to the enhancement of the transverse dispersion. The results of Quintard *et al.* (1997) show a dependence of about 1.3 for a staggered arrangement of cylinders and spheres and 1.7 for in-line arrangement. Their work was restricted to Stokes' flow and the value of 1.3 was ascribed to the enhancement of the transversal dispersion in the staggered arrangement.

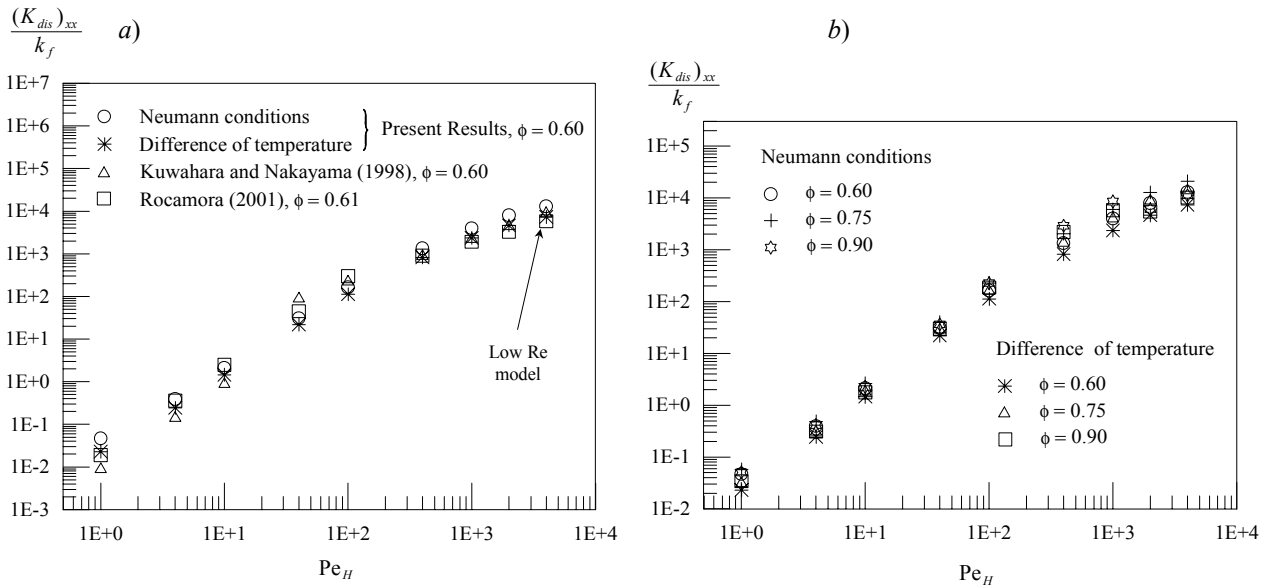


Figure 7. Longitudinal thermal dispersion: a)  $\phi_f = 0.60$  and b) overall results.

The transverse component of the thermal dispersion tensor is shown in Fig. (8) as a function of Peclet number and for different porosities. As can be observed, the use of different temperature boundary conditions (Fig. 2c and Eq.28) yields very little differences in the values of the transverse component. On the other hand, for the transverse component, different morphologies (elliptical, square and cylindrical) yield great differences in its values. Its overall dependence on the Peclet number was  $(K_{dis})_{yy}/k_f = 2.29 \times 10^{-4} Pe_H^{0.88}$ . As expected, this component is much smaller than the longitudinal component for large Peclet numbers.

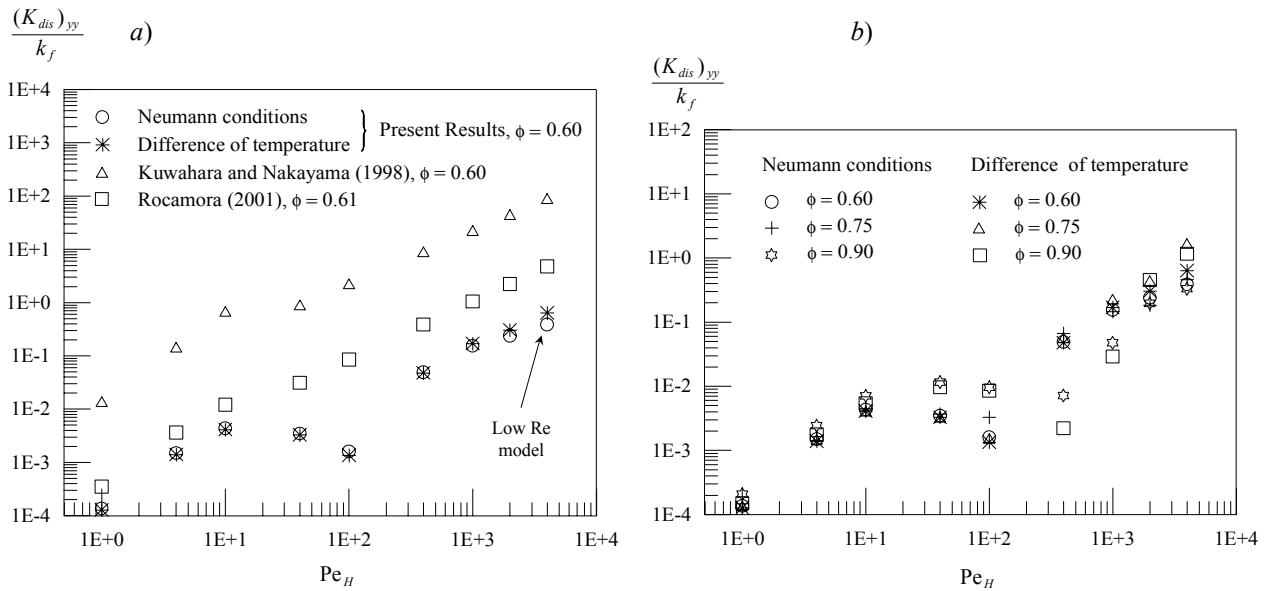


Figure 8. Transverse thermal dispersion: a)  $\phi_f = 0.60$  and b) over all results.

In this work it was talked about three types of approaches to calculate the thermal dispersion tensor. All of them are valid and the question that arises is the validity of using a unit-cell to represent a periodic porous medium in thermal problems. This question will be analyzed using a control volume around the unit-cell as sketched in Fig. (9) and, for a steady state flow and neglecting the viscous dissipation, verifying how the thermal energy enter or exit the unit-cell.

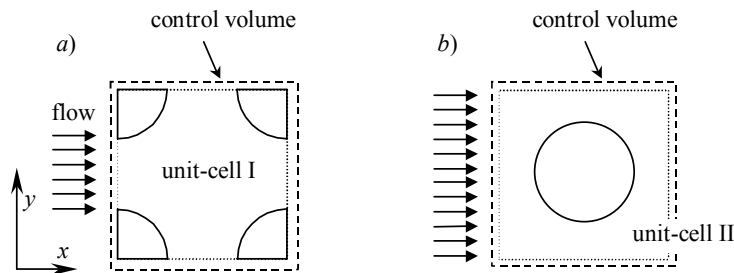


Figure 9. Two types of unit-cell that represent the same periodic porous medium.

Figure (10a) shows the average temperature profile for a periodic porous medium with a difference of temperature imposed from north to south. Independently of the flow rate the gradient of the average temperature will be a constant and transverse to the flow. The energy enters the unit-cell through the north face and exits through south face, not accumulating energy. In this case the problem is "thermally periodic" and the unit-cell, with any of the three types of thermal boundary conditions here discussed, could represent this problem.

In Fig. (10b) we have other case that could be represent by a unit-cell with any of the three types of thermal boundary conditions here discussed. In this case the flow is at rest, the gradient of the average temperature will be a constant and the energy enters the unit-cell through the west face and exits through east face, not accumulating energy. On the other hand, if the flow is not at rest (Fig. 10c) it will enter the unit-cell through the west face with some temperature  $T_1$  and will exit the unit-cell through the east face with a temperature lower than  $T_1$ , *i.e.*, the flow loses energy. Using the control volume sketched in Fig. (9b), this energy can go out of the unit-cell only through north or south faces and, therefore, this problem will not be "thermally periodic" in the  $y$  direction. Actually, the problem as sketched in Fig. (10c) could not occur.

The calculation of the longitudinal thermal dispersion,  $(K_{dis})_{xx}$ , using the unit-cell and boundary conditions as sketched in Fig. (2b), was motivated by the representation of a problem that could occur in a real situation. This problem is described in Fig. (10d) where a uniform heat flux is imposed on north and south faces. Certainly this problem is not "thermally periodic" in the  $y$  direction, but after the thermal entry length it will be "thermally periodic" in the  $x$  direction. The temperature field will increase linearly with  $x$  along the medium and only in the centerline the gradient of the average temperature will be in  $x$  direction, *i.e.*, in the central row of unit-cells, and this is the case here represented in the Fig. (2b).

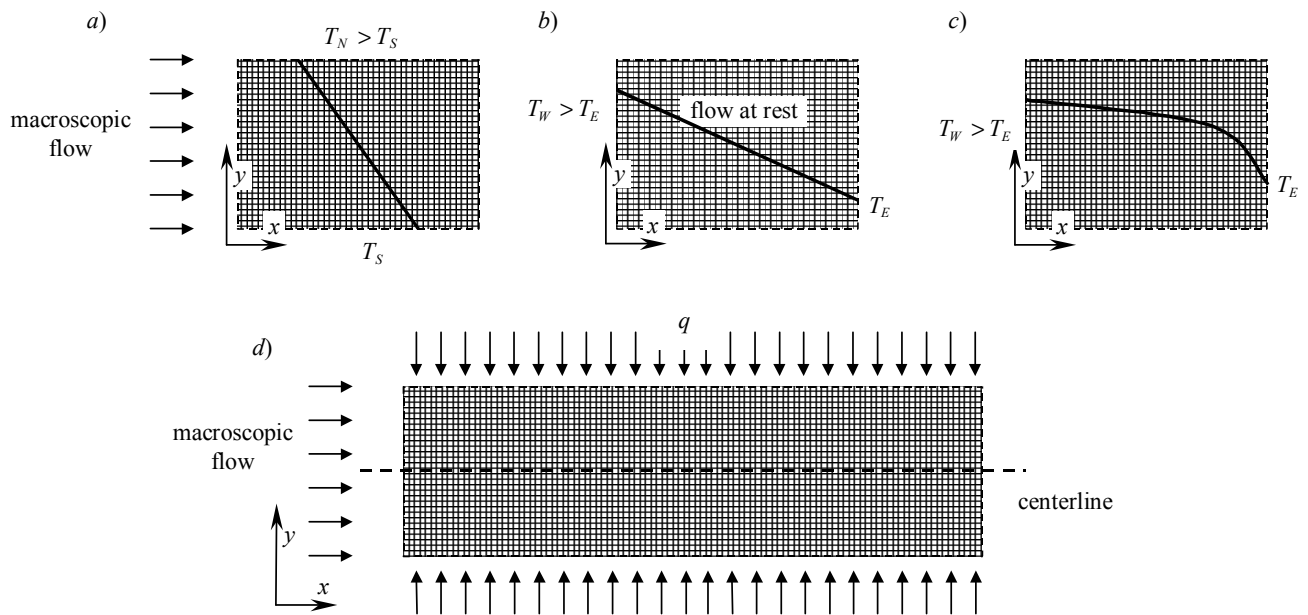


Figure 10. Periodic porous medium: a) flow at rest or convection and difference of temperature from north to south, b) flow at rest and difference of temperature from west to east, c) convection and difference of temperature from west to east, and d) Neumann boundary conditions on north and south faces.

## 6. Conclusions

The modeling of thermal dispersion was discussed and its implication in the determination of the longitudinal and transverse components of the thermal dispersion tensor was presented. Results of thermal dispersion components calculated for a periodic porous medium represented by a unit-cell with Neumann and Dirichlet boundary conditions for the energy equation and periodic boundary condition for mass and momentum equations were presented and compared with data found in the literature. The use of a unit-cell to represent a periodic porous medium in thermal problems was discussed, showing that this approach is valid when the problem in consideration is “thermally periodic” in all directions.

## 7. Acknowledgements

The authors are thankful to FAPESP and CNPq for their financial support during the course of this research.

## 8. References

- Abe, K., Nagano, Y., and Kondoh, T., 1992, An Improved k- $\epsilon$  Model for Prediction of Turbulent Flows with Separation and Reattachment, *Trans. JSME, Ser. B*, vol. 58, pp. 3003-3010.
- de Lemos, M. J. S. and Pedras, M. H. J., 2001, Recent Mathematical Models for Turbulent Flow in Saturated Rigid Porous Media, *ASME Journal of Fluids Engineering*, vol. 123 (4), pp. 935-940.
- Hsu, C. T. and Cheng, P., 1990, Thermal Dispersion in a Porous Medium, *Int. J. Heat Mass Transfer*, vol. 33, pp. 1587-1597.
- Kaviany, M., 1995, *Principles of Heat Transfer in Porous Media*, 2nd edn. Springer, New York.
- Kuwahara, F. and Nakayama, A., 1998, Numerical Modeling of Non-Darcy Convective Flow in Porous Medium, *Proc. of 11th IHTC (Kyongju, Korea)*, vol. 4, pp. 411-416.
- Moyne, C., 1997, Two-Equation Model for a Diffusive Process in Porous Media Using the Volume Averaging Method with an Unsteady-State Closure, *Adv. Water Resour.*, vol. 20 (2-3), pp. 63-76.
- Nakayama, A. and Kuwahara, F., 1999, A Macroscopic Turbulence Model for Flow in a Porous Medium, *ASME Journal of Fluids Engineering*, vol. 121, pp. 427-433.
- Ochoa-Tapia, J. A. and Whitaker, S., 1997, Heat Transfer at the Boundary Between a Porous Medium and a Homogeneous Fluid, *Int. J. Heat Mass Transfer*, vol. 40 (11), pp. 2691-2707.
- Patankar, S. V., 1980, *Numerical Heat Transfer and Fluid Flow*, Hemisphere, New York.
- Pedras, M. H. J. and de Lemos, M. J. S., 2001a, Macroscopic Turbulence Modeling for Incompressible Flow Through Undeformable Porous Media, *Int. J. Heat Mass Transfer*, vol. 44 (6), pp. 1081-1093.
- Pedras, M. H. J. and de Lemos, M. J. S., 2001b, Simulation of Turbulent Flow in Porous Media Using a Spatially Periodic Array and a Low Re Two-Equation Closure, *Numer. Heat Transfer, Part A-Appl*, vol. 39 (1), pp. 35-59.

- Pedras, M. H. J. and de Lemos, M. J. S., 2001c, On Mathematical Description and Simulation of Turbulent Flow in a Porous Medium Formed by an Array of Elliptic Rods, ASME Journal of Fluids Engineering, vol. 123 (4), pp. 941-947.
- Pedras, M. H. J., Rocamora, F. D. and de Lemos, M. J. S., 2003, Simulation of Turbulent Thermal Dispersion in Porous Media Using a Periodic Cell with Prescribed Heat Flux at the Boundaries, Proc. of 3rd Int. Conf.. Computational Heat and Mass Trans., May 26-30, Banff, Canada.
- Pedras, M. H. J. and de Lemos, M. J. S., 2003, Computation of Turbulent Flow in Porous Media Using a Low Reynolds  $k$ - $\epsilon$  Model and an Infinite Array of Transversally Displaced Elliptic Rods, Numer. Heat Transfer; Part A-Appl., vol. 43, n. 6, pp. 585-602.
- Quintard, M., Kaviany, M. and Whitaker, S., 1997, Two-Medium Treatment of Heat Transfer in Porous Media: Numerical Results for Effective Properties, Adv. Water Resour., vol. 20 (2-3), pp. 77-94.
- Rocamora, F.D. and de Lemos, M.J.S., 2000, Analysis of Convective Heat Transfer for Turbulent Flow in Saturated Porous Media, Intern. Comm. Heat and Mass Transfer, vol. 27 (6), pp. 825-834.
- Rocamora, F.D., de Lemos M.J.S. 2002, Numerical Determination Of The Thermal Dispersion Tensor In An Infinite Porous Medium, *Numerical Heat Transfer* (submitted).